Supplementary Methods and Results

Procedure of fMRI and lesion experiments

The task was compiled and run using E-Prime software (Psychology Software Tools, Pittsburgh, PA). Task instructions were first explained to the participants verbally, and then participants performed a practice session on a PC with four runs (one run for each ET condition), using the same number of trials and timing parameters, and an identical button configuration as the actual task. In the fMRI study, once participants demonstrated an understanding of the task, another practice session in an MRI simulator was performed using identical response button gloves as the actual scanner. During the actual scan, stimuli were projected using a liquid crystal display projector (refresh rate: 60 Hz; spatial resolution: 1024 × 768) onto a screen mounted at the back of the magnet bore. A mirror mounted on the head coil was adjusted so that the stimuli appeared in the center of the participants' field of view. MRI-compatible lenses were provided to participants who required their vision to be corrected to normal. Foam padding was used to minimize participants' head movement. Participants' responses were collected using a fiber optic button system (BrainLogic, Psychology Software Tools) with button response gloves placed on participants' left and right hands. Participants made the responses to the stimuli by pressing the buttons under their left and right index fingers for LEFT and RIGHT responses, respectively.

In the lesion study, participants performed the practice session runs (4 runs) and then the testing session runs. They used their right index finger and right middle finger to press the left and right mouse buttons to make left and right responses, respectively.

Demographic information and questionnaire scores in the lesion study groups

The group mean and standard deviation (SD) of the demographic information and questionnaires scores of each group are shown in **Supplementary Table 1.** The differences between each pair of groups were not significant for age (AIC vs. ACC, p = .98; AIC vs. BDC, p = .60; AIC vs. NIC, p = .33; ACC vs. BDC, p = .63; ACC vs. NIC, p = .42; BDC vs. NIC, p = .13), education (AIC vs. ACC, p = .58; AIC vs. BDC, p = .54; AIC vs. NIC, p = .47; ACC vs. BDC, p = .37; ACC vs. NIC, p = .94; BDC vs. NIC, p = .33), MMSE scores (AIC vs. ACC, p = .24; AIC vs. BDC, p = .40; AIC vs. NIC, p = .34; ACC vs. BDC, p = .80; ACC vs. NIC, p = .79; BDC vs. NIC, p > .99), or BDI scores (AIC vs. ACC, p = .42; AIC vs. BDC, p = .30; AIC vs. NIC, p > .99; ACC vs. BDC, p = .10; ACC vs. NIC, p = .36; BDC vs. NIC, p = .37). The difference in chronicity was not significant among patient groups (AIC vs. ACC, p = .14; AIC vs. BDC, p = .59; ACC vs. BDC, p = .63), and the correlation between chronicity and CCC was not significant in all groups (AIC: r = .29, p = .48; ACC: r = .23, p = .66; BDC: r = -.69, p = .059).

Behavioral data analyses

Computing the response accuracy and the reaction time. The analytic procedure for behavioral the data was identical to the one used in our previous study that utilized the full version of the MFT-M (Wu et al., 2016). Trials with no response within the response window were treated as trials with incorrect responses in the analysis of accuracy and were excluded from the analysis of reaction time (RT). Trials with RT exceeding ± 3 SD of the mean RT (across trials in each condition with correct responses) were also removed from the final analysis of RT as outliers. More than 98% trials remained after

this RT trimming (99.1 ± 0.1% in the fMRI study, 99.0 ± 0.5% in AIC group, 99.2 ± 0.3% in ACC group, 98.7 ± 0.6% in BDC group, and 99.1 ± 0.4% in NIC group). For each participant, the mean and SD of RT under each condition were calculated based on these remaining trials. Accuracy for each condition was computed as the percentage of trials with correct responses. For the fMRI study, two 3 (Congruency: 5:0, 4:1, 3:2) × 4 (ET: 250, 500, 1000, 2000 ms) repeated measures ANOVA were conducted on the accuracy and RT separately. Bonferroni correction was used to correct for multiple comparisons in the post-hoc comparisons. For within-subjects designs, error bars in the result figures represented the confidence interval (Cousineau, 2005) in the corresponding condition. Repeated measures ANOVA was not conducted for the behavioral data analysis of the lesions study due to the small sample size.

Estimating the CCC based on the response accuracy. The estimation of the CCC followed the same algorithm as in our previous study (Wu et al., 2016), where we demonstrated that the grouping search is the optimal strategy adopted to determine the direction that the majority of arrows point to, in which participants repeatedly sample stimuli with the majority size (i.e., 3 for the set size of 5) as the sample size. Each sampling is made randomly and independently. A correct response would be made if a congruent sample can be obtained within the ET, otherwise a random guessing response would be made. Therefore, the probability of making a correct response (P_{correct}, equivalent to response accuracy) is:

$$P_{correct} = P_{congruent} \times p_0 + \left(1 - P_{congruent}\right) \times p_{guess} \quad \text{(Equation 1)},$$

in which p_0 is the baseline response accuracy, p_{guess} is the chance level of accuracy for guessing (50%), and $P_{congruent}$ is the probability that at least one congruent sample can be

obtained within a given ET. The $P_{congruent}$ can be calculated as 100% minus the probability that no congruent sample is obtained, which is ${P_{miss}}^{n_s}$, with P_{miss} as the probability of obtaining an incongruent sample by one attempt of search and n_s as the number of attempts. The is P_{miss} determined by the congruency of an arrow set, which can be calculated as

$$P_{miss} = 1 - \frac{C(N_{con}|N_{maj})}{C(N_{size}|N_{maj})} = 1 - \frac{N_{con}!}{(N_{con} - N_{maj})!} \Big/ \frac{N_{size}!}{(N_{size} - N_{maj})!} \qquad \text{(Equation 2).}$$

Here N_{size} is the set size, N_{con} is the number of arrows pointing to the majority direction, and N_{maj} is the majority size. The n_s is determined by the capacity (parameter C) and ET, expressed as $n_s = 2^C \times ET / N_{maj}$. Therefore, for a given parameter C, the estimated response accuracy ($E[accuracy]$) for a given condition can be calculated as

$$E[accuracy] = \left[1 - {P_{miss}}^{\frac{2^C \times ET}{N_{maj}}}\right] \times p_0 + {P_{miss}}^{\frac{2^C \times ET}{N_{maj}}} \times p_{guess} \qquad \text{(Equation 3).}$$

For each participant, the CCC was estimated as the parameter C that provided the best model fitting between empirical and predicted response accuracy across all conditions. The performance of model fitting was evaluated as the likelihood (L) using a binomial likelihood function:

$$L(C) = \prod_i f(i)^{p(i)}(1 - f(i))^{(1-p(i))} \qquad \text{(Equation 4),}$$

where $f(i)$ and $p(i)$ are the empirical and the predicted accuracy, respectively, in condition i. Higher likelihood indicates a better fit to empirical data by the model. For a group of participants, the 95% confidence interval (CI) of the group-mean CCC was estimated by a bootstrapping approach with the bias corrected and accelerated percentile method. The bootstrap samples were generated from the sampling (with replacement) of the CCC values of all participants for 10,000 iterations.

Behavioral results of the fMRI study

The group-mean and SD of response accuracy is shown in **Fig. 2a** and **Supplementary Table 2**. For response accuracy, the main effect of congruency was significant ($F_{2, 52} = 608.93$, $p < .001$), and pair-wise comparisons revealed that response accuracy was significantly different between all congruency conditions (all *ps* < .001), indicating that a decrease in response accuracy was associated with an increase in entropy. The main effect of ET was significant ($F_{3, 78} = 60.44$, $p < .001$), and pair-wise comparisons revealed that accuracy was significantly different between all pairs of ETs (all *ps* < .05), indicating that a decrease in response accuracy was associated with a decrease in ET. The congruency × ET interaction was significant ($F_{6, 156} = 14.11$, $p < .001$), and simple effect analyses showed that the main effect of ET was significant under the 3:2 conditions ($F_{3, 24} = 26.30$, $p < .001$) and the 4:1 conditions, ($F_{3, 24} = 33.17$, $p < .001$), but not significant under the 5:0 conditions ($F_{3, 24} = 1.37$, $p = .27$). These results indicate that for all 5:0 conditions, the response accuracy was approximately 100% and did not change significantly across ETs. For both 4:1 and 3:2 conditions, the response accuracy declined significantly when the ET decreased.

The group-mean and SD of RT is shown in **Fig. 2b** and **Supplementary Table 2**. For the RT, the main effect of congruency was significant ($F_{2, 52} = 351.43$, $p < .001$), and pair-wise comparisons revealed that RT was significantly different between all congruency conditions (all *ps* < .001), with an increase of RT associated with an increase of entropy. The main effect of ET was significant ($F_{3, 78} = 38.12$, $p < .001$), and pair-wise comparisons revealed that RT was significantly different between all ETs (all *ps* < .05), indicating that an increase of RT was associated with an increase of ET. The congruency

× ET interaction was significant ($F_{6, 156} = 57.46$, $p < .001$), and simple effect analyses showed that the main effect of ET was significant under the 3:2 condition ($F_{3, 24} = 36.10$, $p < .001$), the 4:1 condition ($F_{3, 24} = 22.67$, $p < .001$), and the 5:0 conditions ($F_{3, 24} = 5.15$, $p = .007$). These results indicate that the RT increased as a function of ET for all congruency conditions, with the steepness of the RT increase as 3:2 > 4:1 > 5:0. Altogether, our RT findings indicate that the RT increase was not only associated with the increase of entropy, but also constrained by the ET.

GLM results of the fMRI experiment

As shown in **Fig. 3a** and **Supplementary Table 3**, an increase in entropy was associated with a significant increase of activation in all core regions of the CCN, visual areas (including calcarine cortex and mid occipital gyrus), and superior colliculus. It was also associated with a significant decrease of activation in all regions of the default mode network (DMN), including the posterior cingulate cortex (PCC), ventral medial prefrontal cortex (vmPFC), superior frontal gyrus (SGF), mid temporal gyrus (MTG), angular gyrus (ANG), and hippocampus. All activated and deactivated regions were distributed in the two hemispheres symmetrically. As shown in **Fig. 3b** and **Supplementary Table 4**, an increase of the reciprocal of ET (i.e., a decrease in ET) was also associated with a significant increase of activation in all core regions of the CCN and visual areas, and a significant decrease of activation in some regions of the DMN, including the left ANG, left SFG, and left vmPFC. Here the increase and decrease of activation is in terms of the changes of HRF amplitude.

Model fitting for the relationship between the neural involvement and cognitive load

In the following fitted models, *Y* denotes the regional activation of each ROI and *I* denotes the cognitive load (i.e., information rate). For the statistics of model fitting, a better model fitting can be indicated by a smaller value of residual, log-likelihood (logL), Akaike information criterion, or Bayesian information criterion (BIC). Compared to residual and logL that only evaluate the fitting between empirical and fitted data, the Akaike information criterion takes both fitting and the number of estimated parameters into account, and the BIC additionally takes the number of data points into account. In our study, the number of estimated parameters was different between the logistic model (3 parameters) and the linear model (2 parameters), while the number of data points was the same. Therefore, both Akaike information criterion and BIC can be good indexes for our model comparison.

For the left AIC, the fitted linear function was $Y = 0.68 + 0.27\ I$, with root mean squared residual (rmse) = 0.85, logL= -477.1, Akaike information criterion = 964.2, BIC = 970.3. The fitted logistic function was $Y = 0.08 + 6.51(1 - e^{-0.08I})$, with rmse = 0.86, logL= -468.1, Akaike information criterion = 950.6, BIC = 958.9. For the right AIC, the fitted linear function was $Y = 0.76 + 0.24\ I$, with rmse = 0.90, logL= -487.5, Akaike information criterion = 985.0, BIC = 991.1. The fitted logistic function was $Y = 0.14 + 5.53(1 - e^{-0.09I})$, with rmse = 0.91, logL= -479.4, Akaike information criterion = 972.8, BIC = 981.1. In summary, the logistic model fitted the empirical data better compared to the linear model for both left and right AIC, indicated by their smaller logL, Akaike information criterion, and BIC, although the residuals were similar.

For the left ACC, the fitted linear function was $Y = 1.14 + 0.32\ I$, with rmse = 1.19, logL= -579.9, Akaike information criterion = 1169.8, BIC = 1175.9. The fitted logistic function was $Y = 0.32 + 7.32(1 - e^{-0.09I})$, with rmse = 1.27, logL= -576.3, Akaike information criterion = 1166.7, BIC = 1174.9. Although the smaller logL, Akaike information criterion, and BIC indicated that the logistic model fit the empirical data better compared to the linear model, the differences between the two models were very subtle. In addition, the rmse were smaller for the logistic model. Therefore, the linear model, which is simpler than the logistic model, was preferred for the left AIC.

For the right ACC, the fitted linear function was $Y = 0.59 + 0.20\ I$, with rmse = 0.90, logL= -451.3, Akaike information criterion = 912.5, BIC = 918.4. The fitted logistic function was $Y = 0.33 + 6.30(1 - e^{-0.48I})$, with rmse = 1.16, logL= -490.2, Akaike information criterion = 994.4, BIC = 1002.4. Therefore, the linear model fit the empirical data better compared to the logistic model, consistently indicated by its smaller residual, logL, Akaike information criterion, and BIC.

Testing the correlation between CCC and parameter estimates of the capacity-limited model of the right AIC

The correlations between the CCC and parameter estimates of capacity-limited model of the right AIC activation were not significant (span: $r = .21$, $p = .30$, $BF_{10} = 0.26 < 1/3$; baseline activation and half-time: $rs = 0$ because of the insignificant random effects for these two estimates). The prediction of the CCC by the superadditive effect in activation in the right AIC could not be significantly improved by adding additional

regressors (i.e., span, baseline activation, and half-time in the right AIC), $\Delta R^2 = .24$, $\Delta F_{4, 21} = .148 < 1$, indicating that the super-additive effect is the most decisive feature.

Testing the correlation between CCC and grey matter volumes in AIC

To examine the potential association between participants' anatomical structure of the brain and their CCC, we conducted a whole-brain voxel-wise group regression analysis on the grey matter volume images, using their CCC as the regressor. The grey matter volume image of each participant was generated using the VBM8 toolbox (http://dbm.neuro.uni-jena/vbm). The T1-weighted image of each participant was first segmented into six tissue classes (i.e., grey matter, white matter, cerebrospinal fluid, bone, non-brain soft tissue, and air outside of the head and in nose, sinus and ears). The segmented grey matter images were spatially normalized using the 'IXI500_MNI152' template. The modulated normalized images (representing relative volume corrected for brain size) were generated by correcting for non-linear warping of spatial normalization effect, which represents the relative volume after correcting for different brain size. The image for relative grey matter volume for each participant was then spatially smoothed with a Gaussian kernel of 8 mm full-width half-maximum. Second-level group regression analysis was conducted on the smoothed grey matter volume images. All steps used the default parameters in SPM. In addition, the grey matter volume of the right AIC cluster (defined by the super-additive effect of activation) was extracted for each participant. The Pearson correlation efficient (two-tailed) between the right AIC grey matter volume and participants' CCC was calculated. We did not find any significant correlation between the grey matter volumes of any voxel/region under current statistic threshold ($p < .001$).

Participants' CCC was not significantly correlated to the grey matter volume of the right AIC (r = .24, p = .22) or to the left AIC (r = .02, p = .91). These results indicated that the grey matter volume of the AIC was not associated with the individual difference of the CCC.

Results of the mediation analyses

We tested whether the supper-additive activation in the right AIC mediated the relationship between CCC and subscales of the IQ. Beside the significant correlation between the supper-additive activation in the right AIC and the CCC, the Symbol search sub-index was significantly predicted by the super-additive activation in the right AIC (R^2 = .24, $F_{1, 25}$ = 8.06, B = 0.56, p = .009), and by the CCC (R^2 = .48, $F_{1, 25}$ = 23.22, B = 3.35, p < .001). In the model with super-additive activation in the right AIC and CCC as the predictors, and Symbol search sub-index as the target variable (R^2 = .50, $F_{2, 26}$ = 11.98, p < .001), the coefficient was significant for the CCC (B = 3.50, p = .002) but not for the super-additive activation in the right AIC (B = 0.181, p = .362), indicating that the superadditive activation in the right AIC was not a mediator for the relationship between CCC and Symbol search sub-index.

The Vocabulary sub-index was significantly predicted by the super-additive activation in the right AIC (R^2 = .18, $F_{1, 25}$ = 5.57, p = .026) but not by the CCC (R^2 = .08, $F_{1, 25}$ = 2.16, p = .155), while the Figure Weight sub-index could not be significantly predicted by either the super-additive activation in the right AIC (R^2 = .06, $F_{1, 25}$ = 1.65, p = .211) nor by the CCC (R^2 = .002, $F_{1, 25}$ < 1). These results indicate that the super-

additive activation in the right AIC was not a mediator for the relationship between the CCC and either of these two sub-indices.

Connection changes in networks with simulated lesion

To identify the connections with significant changes after the simulated AIC and ACC lesions, we conducted pairwise *t*-tests (two-tailed) to compare the connectivity between the networks with and without a simulated lesion, and found that the corresponding contralateral region showed significant increase in connectivity (**Supplementary Fig. 7**).

Supplementary References

Cousineau, D., 2005. Confidence intervals in within-subject designs: A simpler solution to Loftus and Masson's method. Tutor Quant Methods Psychol 1, 42-45.

Wu, T., Dufford, A.J., Mackie, M.-A., Egan, L.J., Fan, J., 2016. The capacity of cognitive control estimated from a perceptual decision making task. Sci Rep 6, 34025.

Supplementary Tables

Supplementary Table 1. Characteristics of participants in the lesion study.

Group	N	Laterality	Chronicity (months) [a]	Age (years)	Gender	Education (years)	MMSE	BDI
AIC	8	2L/6R	21.2 (11.1)	38.9 (9.4)	3F/5M	12.9 (2.3)	27.6 (1.5)	2.1 (1.8)
ACC	6	3L/3R	16.9 (18.4)	36.0 (8.8)	2F/4M	11.3 (5.4)	28.4 (1.1)	3.7 (3.0)
BDC	8	N/A	12.6 (8.4)	39.0 (11.0)	4F/4M	13.8 (3.4)	28.5 (1.2)	3.1 (2.7)
NIC	27	N/A	N/A	42.7 (9.2)	15F/12M	13.7 (2.0)	28.2 (1.8)	2.1 (1.8)

Note: Errors (in parenthesis) represent the standard deviation (SD) of the mean reaction times across participants in the corresponding group. N: number of participants in the final sample. MMSE: Mini-Mental State Examination scores. BDI: Beck Depression Inventory scores. AI: anterior insular cortex focal lesion group. AIC: anterior insular cortex focal lesion group. ACC: anterior cingulate cortex focal lesion group. BDC: brain damage control group, including patients with lesion in regions outside CCN. NIC: neurologically intact participants. L: lesion in left hemisphere. R: lesion right hemisphere. F: female; M: male. N/A: not available. [a] Chronicity: period of time between surgery and testing.

Supplementary Table 2. Mean (SD) of response accuracy and reaction time (RT) in each condition of the fMRI study.

		ET (ms)			
	Congruency	250	500	1000	2000
Accuracy (%)	5:0	98.7 (2.5)	99.4 (1.4)	99.2 (1.5)	99.7 (0.9)
	4:1	85.2 (7.7)	90.5 (7.3)	94.1 (5.7)	98.4 (2.3)
	3:2	60.4 (7.5)	63.9 (8.9)	72.3 (10.1)	79.7 (10.9)
RT (ms)	5:0	665 (104)	718 (142)	746 (125)	762 (119)
	4:1	791 (136)	922 (155)	1042 (154)	1137 (169)
	3:2	888 (178)	1053 (194)	1239 (185)	1425 (217)

Note: SD: standard deviation. ET: exposure time.

Supplementary Table 3. Brain regions showing positive/negative activation for the main effect of information entropy.

Regions	L/R	BA	x	y	z	T	Z	K
Positive								
Anterior insular cortex	L		-28	28	-4	13.21	7.23	1076
Anterior insular cortex	R		32	26	-6	12.56	7.07	1119
Anterior cingulate cortex[a]	R	32	4	26	40	11.65	6.84	4593
Inferior frontal gyrus	L	44	-42	2	28	7.99	5.63	
Superior frontal gyrus[b]	L	6/8	-26	0	58	6.48	4.96	
Inferior frontal gyrus	R	44	42	12	28	10.33	6.46	2027
Mid frontal gyrus[b]	R		30	4	56	8.41	5.80	
Inferior frontal gyrus	R	6/8	50	36	26	4.35	3.73	
Postcentral gyrus	R	2	46	-30	46	9.53	6.20	2516
Inferior parietal lobule	R	7/40	28	-52	50	7.52	5.43	
Mid occipital gyrus	R	19	30	-68	28	6.52	4.97	
Superior colliculus	R		6	-22	-10	8.26	5.74	2346
Caudate nucleus[c]	L		-8	10	4	8.26	5.73	
Superior colliculus	L		-4	-24	-12	7.62	5.48	
Caudate nucleus[c]	R		12	8	2	7.26	5.32	
Thalamus	L		-10	-8	4	7.18	5.28	
Thalamus	R		10	-10	2	6.64	5.03	
Inferior parietal lobule	L	7/40	-30	-46	44	7.93	5.61	2237
Mid occipital gyrus	L	19	-26	-68	30	6.78	5.10	
Calcarine cortex	R	17	14	-72	10	5.45	4.41	310
Calcarine cortex	L	17	-12	-72	10	5.41	4.39	413
Negative								
Angular gyrus	R	39	50	-60	34	8.29	5.75	851
Superior frontal gyrus	R	9	16	42	38	7.26	5.32	6535
Superior frontal gyrus	L	9	-18	30	42	7.23	5.31	
Superior frontal gyrus (medial)	L	10	-8	64	4	6.51	4.97	
Orbitofrontal cortex	R	11	2	40	-12	6.28	4.85	
Mid temporal gyrus	R	21	62	-6	-18	6.73	5.08	6424
Rolandic operculum	R		46	-6	12	6.62	5.02	
Hippocampus	R	34	30	-12	-22	6.40	4.92	
Posterior cingulate cortex	R	23	16	-32	40	6.19	4.81	
Supramarginal gyrus	R	40	54	-24	26	5.60	4.50	
Mid cingulate cortex	L	23	-6	-22	40	5.18	4.26	
Posterior cingulate cortex	L	23	-2	-48	32	5.06	4.18	
Superior temporal gyrus	R	22	64	-34	4	4.58	3.88	
Mid temporal gyrus	L	21	-54	4	-26	6.72	5.07	488
Angular gyrus	L	39	-48	-66	36	6.62	5.02	1085

Rolandic operculum	L		-42	-12	22	6.36	4.89	2469
Supramarginal gyrus	L	40	-60	-28	28	5.19	4.26	
Hippocampus	L	34	-28	-22	-16	5.63	4.51	531

Note: Regions are listed in a descending order by their peak Z value. For a cluster with multiple local peaks, the number of voxels in the whole cluster was only listed under the first local peak (also for other activation tables). The threshold was $p < 0.001$ ($T > 3.43$) for the height and $p < 0.006$ ($k > 185$ of $2 \times 2 \times 2$ mm voxels) for the extent, resulting in a corrected threshold of cluster level $p < 0.05$.
L: left; R: right. BA: Brodmann area. [a] Extending to right anterior cingulate cortex. [b] Including frontal eye field (FEF). [c] Extending to putamen.

Supplementary Table 4. Brain regions that showed positive/negative activation for the main effect of the reciprocal of exposure time (1/ET).

Regions	L/R	BA	x	y	z	T	Z	K
Positive								
Anterior insular cortex	L		-32	20	2	9.30	6.12	33350
Inferior parietal lobule	L	7/40	-30	-50	52	9.14	6.07	
Inferior frontal cortex	R	44	46	10	28	8.82	5.95	
Fusiform gyrus	L	37	-42	-66	-4	8.79	5.94	
Anterior insular cortex	R		32	20	0	8.57	5.86	
Mid occipital gyrus	L	19	-26	-70	30	8.56	5.85	
Hippocampus	R	34	26	-24	-8	8.33	5.76	
Mid insular cortex	L		-38	-2	12	8.24	5.73	
Mid occipital gyrus	R	19	32	-66	34	8.01	5.64	
Lingual gyrus	R	18	18	-88	-6	7.89	5.59	
Inferior parietal lobule	R	7/40	36	-44	56	7.77	5.54	
Cerebellum IV/V	L		-8	-48	-14	7.66	5.49	
Superior frontal gyrus[a]	R	6/8	32	-2	52	7.51	5.43	
Anterior cingulate cortex[b]	L	32	2	26	42	7.46	5.41	
Fusiform gyrus	R	37	42	-58	-10	7.42	5.39	
Hippocampus	L	34	-22	-24	-6	7.34	5.36	
Lingual gyrus	L	18	-18	-90	0	7.34	5.35	
Postcentral gyrus	R	3	50	-24	48	7.32	5.35	
Cerebellum I	L		-10	-74	-28	6.77	5.09	
Cerebellum VI	L		-34	-58	-26	6.66	5.04	
Superior colliculus	L		-8	-24	-14	6.57	5.00	
Superior colliculus	R		8	-26	-4	6.23	4.83	
Cerebellum IV/V	R		16	-46	-20	6.25	4.84	
Cerebellum VI	R		16	-70	-24	6.14	4.78	
Caudate nucleus[c]	L		-10	8	-4	6.06	4.74	
Calcarine cortex	R	17	12	-66	14	5.75	4.58	
Thalamus	L		-6	-14	12	5.47	4.42	
Thalamus	R		18	-10	10	5.43	4.40	
Caudate nucleus[c]	R		12	10	-8	5.38	4.37	
Superior frontal gyrus[a]	L	6/8	-30	-2	62	4.97	4.13	
Mid occipital gyrus	R	19	40	-82	8	4.55	3.87	
Supplementary motor cortex	L	6	-4	0	60	4.24	3.67	
Retrosplenial cortex	R	29	6	-24	30	6.34	4.88	284
Superior temporal gyrus[d]	R	42	54	-42	16	5.43	4.40	176
Negative								
Angular gyrus	L	39	-46	-72	36	6.63	5.03	461
Superior frontal gyrus	L	9	-26	22	44	5.17	4.25	175
Superior frontal gyrus (medial)	L	10	-12	60	12	5.15	4.23	180

Orbitofrontal cortex	L	11	-2	56	-12	4.99	4.14	348

Note: The threshold was $p < 0.001$ ($T > 3.43$) for the height and $p < 0.004$ ($k > 142$ of $2 \times 2 \times 2$ mm voxels) for the extent, resulting in a corrected threshold of cluster level $p < 0.05$.

[a] Including frontal eye field (FEF). [b] Extending to right anterior cingulate cortex. [c] Extending to putamen. [d] Temporoparietal junction.

Supplementary Table 5. Brain regions that showed positive/negative activation for the information entropy × reciprocal of ET interaction.

Regions	L/R	BA	x	y	z	T	Z	K
Anterior insular cortex	R		32	26	-8	7.61	5.47	426
Anterior cingulate cortex[a]	R	32	8	28	38	7.17	5.28	667
Anterior insular cortex	L		-32	22	0	6.19	4.81	442
Inferior parietal lobule	L	40	-28	-48	44	4.95	4.12	221

Note: The threshold was $p < 0.001$ ($T > 3.43$) for the height and $p < 0.127$ ($k > 47$ of $2 \times 2 \times 2$ mm voxels) for the extent, resulting in a corrected threshold of cluster level $p < 0.05$. [a] Extending to left anterior cingulate cortex.

Supplementary Table 6. Global efficiency changes in networks with simulated lesion.

		Mean	SE	*p*
Simulated lesion	Non-lesion	0.210	0.012	
	L AIC	0.185	0.002	< .001
	R AIC	0.185	0.012	< .001
	L ACC	0.190	0.011	< .001
	R ACC	0.191	0.011	< .001
	L FEF	0.163	0.010	< .001
	R FEF	0.182	0.010	< .001
	L IPS	0.184	0.008	< .001
	R IPS	0.188	0.010	< .001
	L TH	0.186	0.010	< .001
	R TH	0.188	0.011	< .001
	L CdN	0.189	0.010	< .001
	R CdN	0.189	0.011	< .001
	L V	0.193	0.010	< .001
	R V	0.193	0.011	< .001

Note: L: left, R: right. AIC: anterior insula cortex. ACC: anterior cingulate cortex. FEF: frontal eye field. IPS: area near and along the intraparietal sulcus. TH: thalamus. CdN: caudate nucleus. V: visual areas including calcarine cortex extending to mid occipital gyrus.

Supplementary Figures

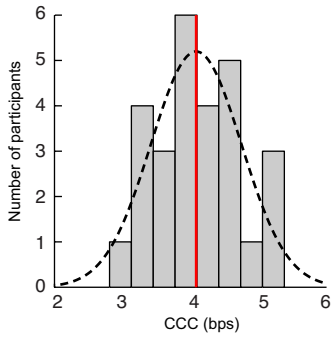

Supplementary Figure 1. Histogram of the estimated capacity of cognitive control (CCC). bps: bit per second. Red vertical line indicates the group mean of CCC. Dashed curve represents fitted normal distribution.

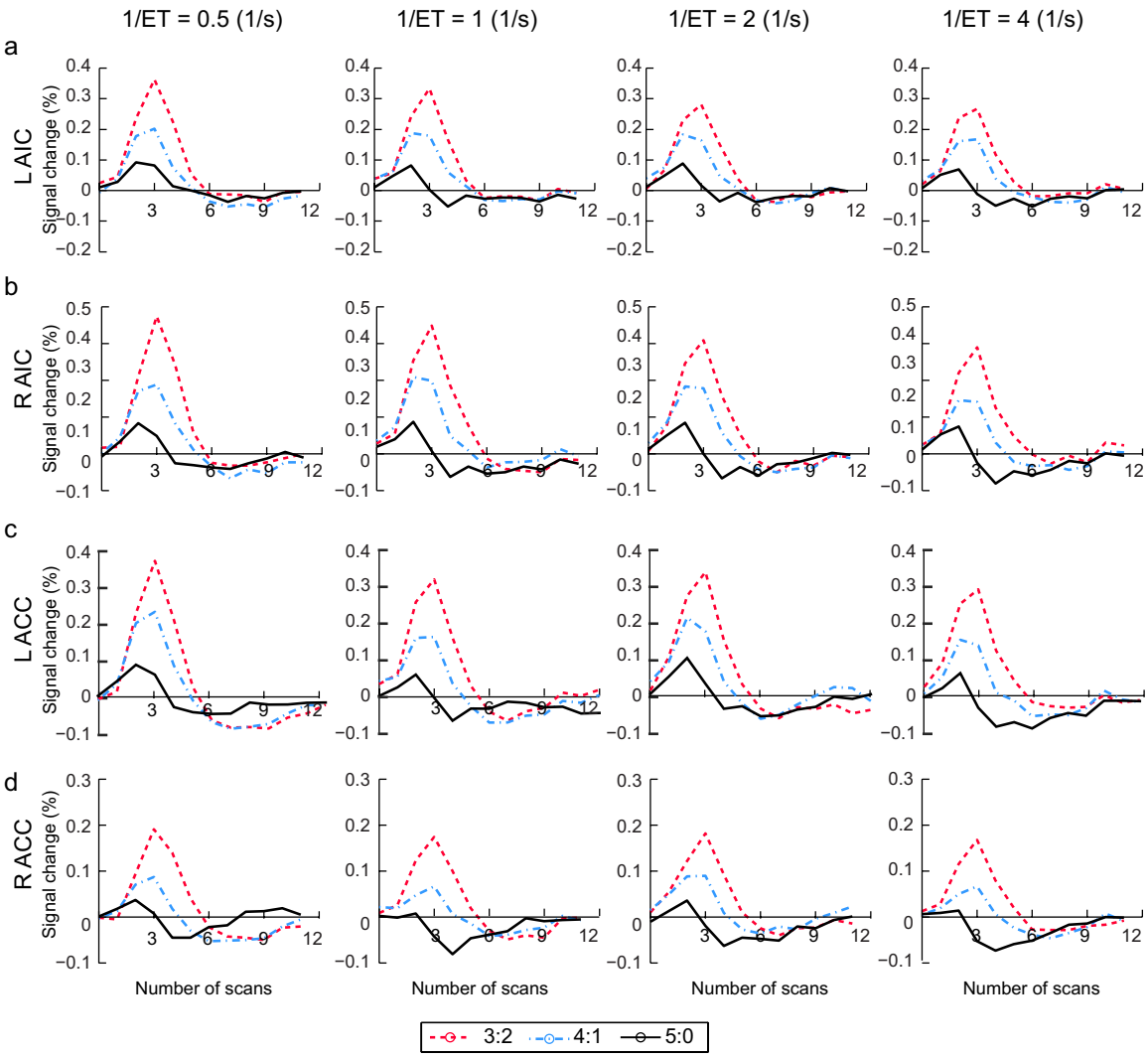

Supplementary Figure 2. Cumulative hemodynamic response curves in each task condition for regions showing a significant positive effect in the conjunction.

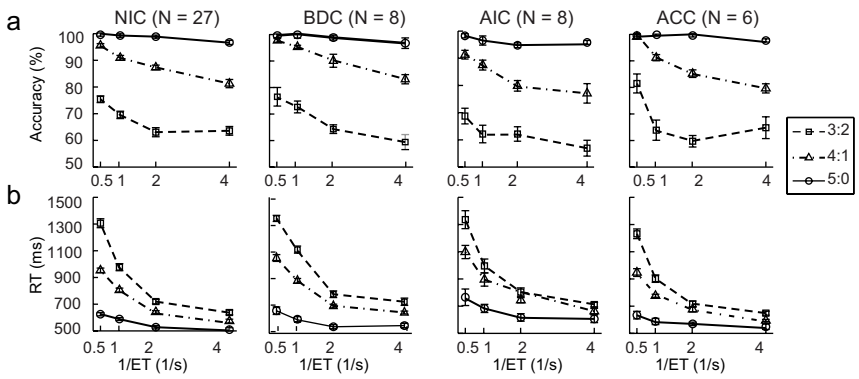

Supplementary Figure 3. Behavioral performance in each group of the lesion study. (a) Response accuracy. (b) Reaction time (RT). NIC: neurologicallly intact control. BDC: brain damage control. AIC: patients with unilateral focal lesion of the AIC. ACC: patients with unilateral focal lesion of the ACC. Error bars indicate SE for within-subject design.

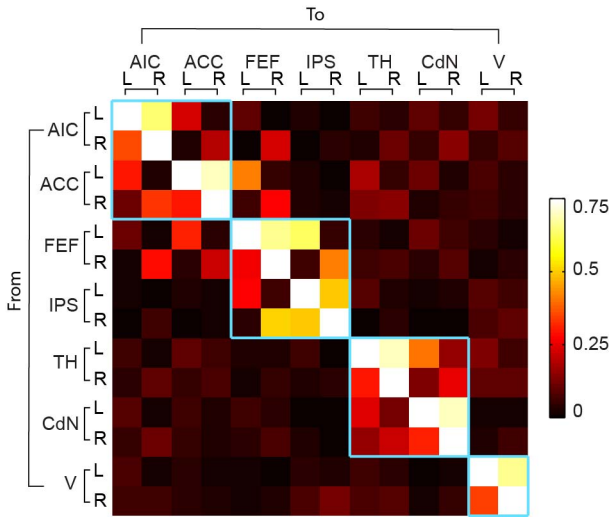

Supplementary Figure 4. Connectivity matrix of the non-thresholded group-averaged Bayesian network. Color bars indicate the coding to the connectivity in the color map, with brighter colors for stronger connectivity. Light blue lines indicate the boundary of each module of the estimated community structure.

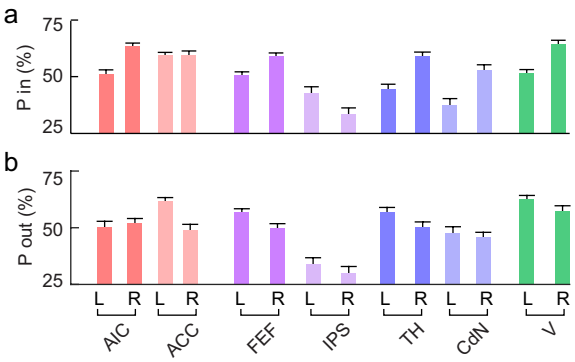

Supplementary Figure 5. Participation coefficient for each region of the CCN. (a) Participation coefficient for inward connections (P in). (b) Participation coefficient for outward connections (P out).

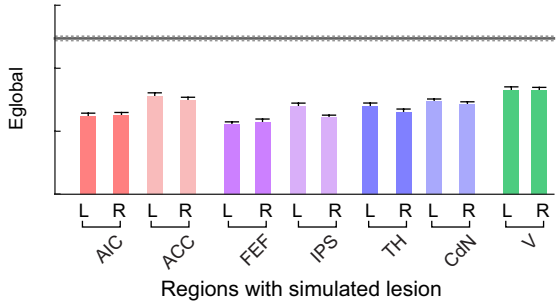

Supplementary Figure 6 Global efficiency (E_{global}) of networks with simulated unilateral lesion. The grey line represents the mean (solid line) and standard error (dashed lines) of the E_{global} of the non-lesioned network.

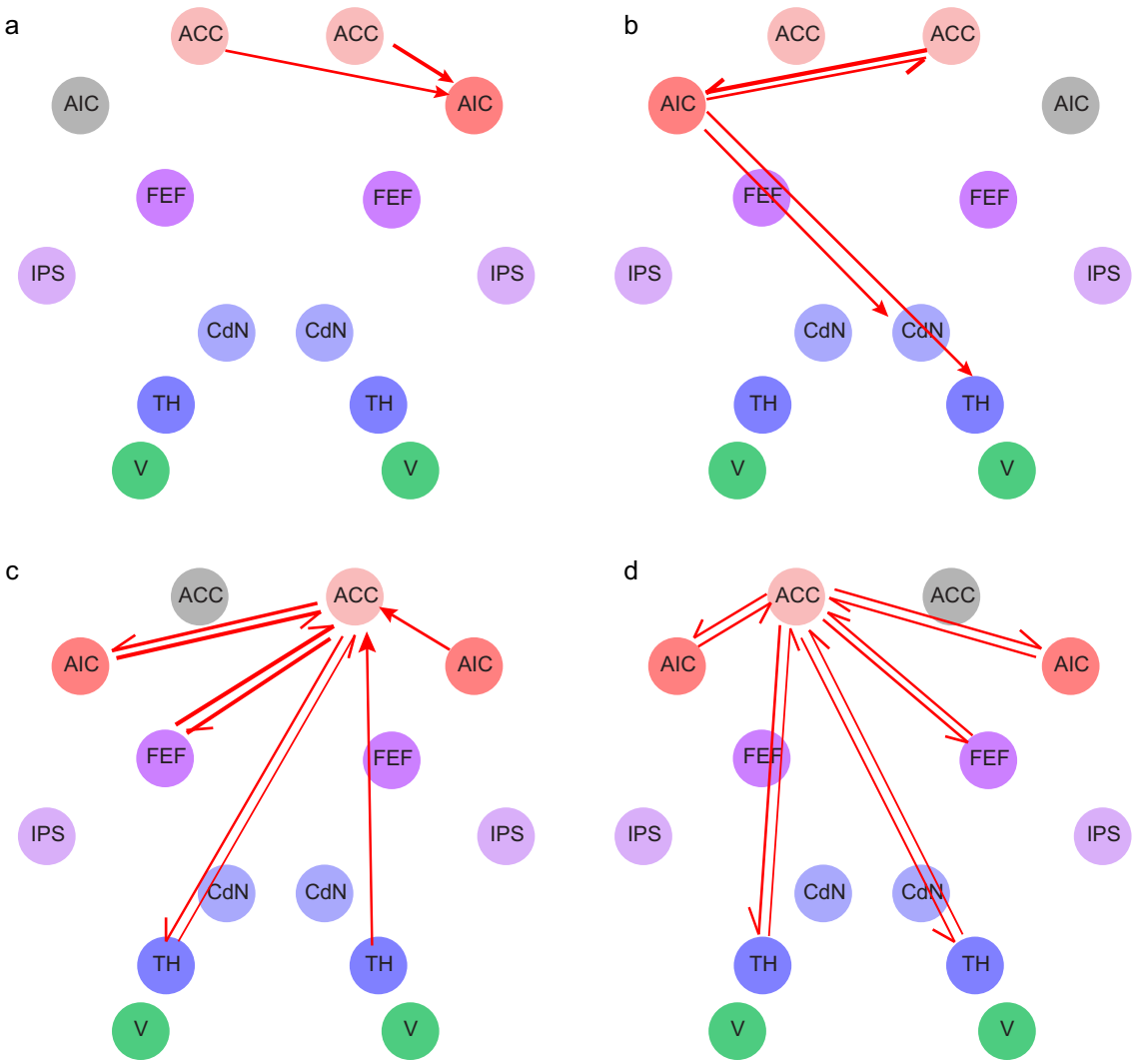

Supplementary Figure 7. Connections showing significant changes for networks with simulated lesion. The grey circles indicate nodes with simulated lesions. arrows: connections with significantly increased. No connection with significantly decreased connectivity was found. (a) Left AIC lesion. (b) Right AIC lesion. (c) Left ACC lesion. (d) Right ACC lesion.